Ceramics International 50 (2024) 27139–27146

Contents lists available at ScienceDirect

Ceramics International

journal homepage: www.elsevier.com/locate/ceramint

Apatite–Wollastonite (AW) glass ceramic doped with B_2O_3: Synthesis, structure, SEM, hardness, XRD, and neutron/charged particle attenuation properties

Khadijah Mohammedsaleh Katubi [a], Erhan Ibrahimoglu [b], Fatih Çalışkan [b], Z.A. Alrowaili [c], I.O. Olarinoye [d], M.S. Al-Buriahi [e,*]

[a] Department of Chemistry, College of Science, Princess Nourah bint Abdulrahman University, P .O. Box 84428, Riyadh, 11671, Saudi Arabia
[b] Department of Metallurgical and Materials Engineering, Faculty of Technology, Sakarya University of Applied Sciences, Sakarya, Turkey
[c] Department of Physics, College of Science, Jouf University, P.O. Box:2014, Sakaka, Saudi Arabia
[d] Department of Physics, School of Physical Sciences, Federal University of Technology, Minna, Nigeria
[e] Department of Physics, Sakarya University, Sakarya, Turkey

ARTICLE INFO

Handling Editor: Dr P. Vincenzini

Keywords:
Apatite–Wollastonite
Glass ceramics
Neutrons
Particle beam
Solid state reaction

ABSTRACT

In the study, the influence of doping apatite-wollastonite (AW) glass-ceramics (GCs) with B_2O_3 on the structural, physical, microstructural, and light and heavy particle interaction properties is presented. Using the solid-state reaction and the cold isostatic press method, pristine AW, 10 wt% (AW-B10), and 20 wt% (AW-B20) B_2O_3-doped AW GCs were prepared. The prepared GCs were subject to structural, chemical compositional, and surface morphological investigation through standard experimental processes. Furthermore, the neutron (fast and thermal) and charged radiation (electron, proton, alpha, and carbon ion) interactional parameters of the GCs were obtained through standard theoretical models and software. The density of AW (2.91 gcm^{-3}) increases to about 2.957 and 2.986 gcm^{-3} as B_2O_3 increases to 10 and 20 wt%, respectively. The presence of boron oxide supported the wollastonite phase to remain glass and suppressed crystallisation in the AW GCs. Doping AW with B_2O_3 improved the interaction probabilities of the GCs with fast and thermal neutrons, electrons, protons, alpha particles, and carbon ions. B-rich AW is thus potentially useful as a target material in human tissues for boron neutron capture therapy for the management of cancer and tumours, isolating or shielding specific tissues in ion beam therapy processes, and other techniques that require the exposure of human tissues to irradiation.

1. Introduction

Synthetic biomaterials such as glasses and ceramics have become essential resources in biomedical processes involved in the management of human tissues and organ impairments. Common among these applications are tissue regeneration and engineering, dental care and corrections, stimulation of growth in bones, and replacement of bone tissues [1–4]. In the past, different glass-ceramics (GCs), such as synthetic hydroxyapatite (SHA) and calcium-phosphate based ceramics, have been successfully used in bone engineering, among others. The SHA is particularly popular in clinical practices due to the similarity between its chemical composition and the inorganic content of bone tissues since HA is the major composite of human bone [5]. The osteo-inductive, osteogenic, and osteoconductive attributes of SHA are responsible for its wide application as a bonding agent for dental and bone reformations [3,6]. In addition, SHA has also been adopted as a courier to deliver therapeutic materials such as drugs, proteins, and genes to target tissues [6,7]. Despite its properties and success as a biomaterial, the bioactivity, mechanical strength, and associated attributes of SHA have been found to be second best to those of apatite-wollastonite (AW) glass ceramic [8].

Apatite-wollastonite (AW) glass ceramics were first developed by Kokubo et al. in 1982 [9,10]. This novel material (as it were) contains the crystal phase of wollastonite and apatite within a glassy structure. Compared to other bioglasses and ceramics such as the SHA, the AW GCs have higher bioactivity and are osteoconductive [8]. It has been reported that AW GCs can withstand up to 65 MPa stress in a biological environment for a period spanning over a decade [9]. Thus, AW GCs are

* Corresponding author.
E-mail address: mohammed.al-buriahi@ogr.sakarya.edu.tr (M.S. Al-Buriahi).

https://doi.org/10.1016/j.ceramint.2024.05.011
Received 13 November 2023; Received in revised form 2 March 2024; Accepted 2 May 2024
Available online 9 May 2024

increasingly being used in clinical processes for different functionality. Apatite-wollastonite (AW) glass ceramics are commercially available in powder or bulk forms for applications and studies. However, the powder form is a homogeneous mixture of apatite and wollastonite crystalline phases, unlike the bulk form, which often cracks due to the presence of the crystal phases.

Due to the importance of AW GCs, different preparatory routes have been used to fabricate them. Also, the role of diverse modifying agents in influencing their useful properties has been investigated. Similar to glasses and ceramics, altering the chemical composition of AW would absolutely influence its properties and functionality. The bioactivity, stability, physical attributes, and tissue-bonding properties of AW GCs have been altered when the composition stoichiometry is changed [11–13]. Research has also suggested that an increase in the crystallinity of AW GC can affect its bioactivity [14]. In 2020, Melo et al. showed that doping AW with Al_2O_3 (0.14–0.68 wt%) improved thermal stability, lowered density, and crystallized the GCs [15]. Jing et al. [16] have also reported that when doped with Ti, AW GC had enhanced mechanical features, stability, and bioactivity. Ti-doped AW was thus recommended as a good biomaterial for orthopaedical functions. Obviously, the bioactivity and essential attributes of AW GCs can be improved when the right modifier ions in the right quantity are introduced to the GC system.

B_2O_3 is a glass-forming oxide whose glass-forming ability can be improved through the addition of modifying oxides or other glass-forming oxides. Due to its low melting point, B_2O_3 is sometimes used as a fluxing agent for reducing the sintering and melting temperatures of ceramics [17]. Boron-rich bioactive glasses have shown remarkable attributes compared to their boron-deficient counterparts. For instance, Yan et al. [18] showed that the addition of B_2O_3 has a significant impact on the general properties of CaO + SiO_2+P_2O_5 bioactive GCs. The melting temperature was lowered from 1050C to 950C when the borate content increased from 0 to 20 mol% without significantly altering the bioactivity of the glass system. The mechanical strength was also reported to be enhanced by borate introduction. Similar benefits of B_2O_3 in other bioactive glass systems have also been reported [19–21]. Consequently, the introduction of B_2O_3 into the structure of AW GCs could be desirable based on the aforementioned studies.

The use of radiation and isotopes for therapeutic purposes is well known. Radiation can be delivered into tissues using external or internal beam sources. In brachytherapy, the source of radiation can be kept inside the patient for long or short periods, depending on the dose rate and medical condition. The traditional brachytherapy source includes seeds of radiation sources encapsulated and implanted inside the patients. This method requires at least two surgical procedures: first, to insert and second, to remove the source capsule after the treatment procedure. These can be expensive and also cause patients some discomfort. To address this issue, compatible bioactive GCs could be inserted and activated to serve as the source of radiation. AW GCs doped with B_2O_3 could be an ideal material for the target radiotherapy procedure. First, boron has a strong affinity for neutrons; this boron-rich GC can be used to control the neutron activation process. Second, the boron content could serve as the target nucleus to initiate boron-neutron capture therapy.

In this research, we present the synthesis, structural and microstructural properties, and physical features of AW GCs. Also, neutron, light, and heavy ion cross-section-related parameters are presented in order to understand how boron can be used to improve the radiation absorption ability of AW GCs in brachytherapy and external beam therapy procedures. The light and heavy ions considered are electrons, protons, alpha particles, and carbon ions. These could be primary beams for therapy or secondary knock-on particles in ion beam therapy. The data from this research are significant for assessing the radiation dosimetry properties of the investigated materials. They are also useful for the analysis of the optimum boron concentration for the absorption of neutrons and charged radiation in the AW GCs. This will reveal the possibility of using the synthesized materials as radiation insulators in external (ion or neutron) beam therapy and brachytherapy.

Table 1
The classifications of the samples.

Samples	Codes
AW	Undoped AW Glass Ceramic
AW-B10	10 % B_2O_3 doped AW Glass Ceramic
AW-B20	20 % B_2O_3 doped AW Glass Ceramic

Fig. 1. Fabrication of the samples.

2. Materials and method

In the study, AW glass ceramics doped with different amounts of B_2O_3 were prepared through the solid-state reaction process. The AW was obtained in powder form, while B_2O_3 (purity 99.99 %) was obtained from Merck, Germany. All laboratory wares were cleaned with ethyl alcohol before being used for the GCs preparation. Appropriate proportions of the AW and B_2O_3 powders were mixed according to the composition given in Table 1. The codes AW, AW-B10, and AW-B20 present undoped AW samples, 10 wt% B_2O_3-doped, and 20 wt% B_2O_3 doped AW GCs, respectively. The components were thoroughly mixed using the ball milling process for 30 min for a solid-state reaction to take place and to obtain homogeneous samples. To densify the powder samples, they were poured into steel molds and subjected to a pressure of 225 bar. In addition, using 250 MPa pressure, the cold isostatic press (CIP) process was performed to further densify the samples. The resulting samples were then sintered in an aluminium crucible for 2 h at a temperature of 1000 °C. The summary of the fabrication process of the AW GCs is presented in Fig. 1. The density of each densified AW GC was measured by measuring the mass with an electronic weighing balance and estimating the volume of the regular shaped disc shown in Fig. 1. The density of the prepared material was then obtained by dividing the obtained mass by the estimated volume of the disc. The error ($\Delta\rho$) in the density was computed as:

$$\Delta\rho = \frac{\partial\rho}{\partial m}\Delta m + \frac{\partial\rho}{\partial V}\Delta V \quad (1)$$

where, Δm and ΔV is the error associated with mass and volume, respectively.

Table 2
Sample code and weight fraction (wt.%) of compound present in the prepared AW-*x*B glasses including their measured density.

Composition (wt%)	Glass sample		
	AW	AW-10B	AW-20B
B		3.10571	6.21142
O	41.17605	43.95274	46.72971
F	0.03407	0.03066	0.02725
Mg	1.17592	1.05833	0.94074
Al	1.00558	0.90502	0.80446
Si	15.78995	14.21096	12.63196
P	5.86986	5.28287	4.69610
Ca	34.94858	31.45372	27.95886
Density (±0.002 g/cm^3)	2.905	2.957	2.986

The consequent influence of doping the AW GCs with B_2O_3 on the various properties of the AW samples was investigated as follows: First, the structural integrity of the prepared AW GCs was probed using the X-ray diffraction (XRD) method. Second, the surface morphology and particle distribution were investigated with the aid of a scanning electron microscope (SEM). Third, the electron diffraction spectroscopy was adopted for evaluating the chemical composition of the GCs. Lastly, the relevance of the GCs in attenuating, absorbing, or capturing radiation such as neutrons and charged radiation was evaluated, starting with the computation of parameters linked to the interaction of the different radiation with the GCs. The interaction probability of neutron with GCs was assessed by calculating the fast neutrons (FN) removal cross-section (Σ_R) and the thermal neutron total cross-section (σ_{tot}) and Equations (1) and (2) summarised the computation process [22–25]. The cross-sections measure the probability of neutrons of a particular energy interacting in a certain way in a material. Thermal neutrons can be absorbed or scattered through elastic and inelastic scattering by an interacting medium. The microscopic cross-section σ_j expresses the probability of these interactions taking place within a medium. On the other hand, Σ_R is a measure of how well the material can thermalize fast neutrons after the first collision between atoms of the material and FN.

$$\Sigma_R\left(cm^{-1}\right) = \sum \rho_i * \left(\frac{\Sigma_R}{\rho}\right)_i \tag{2}$$

$$\sigma_{tot} = \sum \sigma_j \tag{3}$$

In Equation (1), ρ_i is the partial density of the chemical elements present within the chemical composition of the GCs, the corresponding FN mass Σ_R of each element is denoted as $\left(\frac{\Sigma_R}{\rho}\right)_i$. Both parameters were estimated directly according to the following expressions:

$$\rho_i = f_i\rho \tag{4}$$

$$\left(\frac{\Sigma_R}{\rho}\right)_i = \begin{cases} 0.19Z^{-0.743}, for\ Z_i \le 8 \\ 0.125Z^{-0.565}, for\ Z_i > 8 \end{cases} \tag{5}$$

where, f_i is the weight proportion of the chemical elements in the GCs with corresponding atomic number Z_i. The measured bulk density of the composite GC sample is represented by ρIn Equation (2), the total thermal neutron (TN) interaction probability for scattering (coherent and incoherent) and absorption, designated as σ_j, were calculated each based on the expression [25]:

$$\sigma_j\left(cm^{-1}\right) = 0.602\rho\sum\frac{f_i}{M_i}\sigma_i \tag{6}$$

where, σ_i and M_i are the cross-sections (for scattering (coherent and incoherent) and absorption) and molar weight of the distinguished elements in the composite GCs.

Also, the stopping power S_p (MeVcm^2/g) and range of electrons, protons, and alpha particles were computed using ESTAR, PSTAR, and ASTAR [26] while those of heavy carbon ions[27,28] were obtained from SRIM Monte Carlo calculations [29]. The range and stopping powers were estimated for particles having kinetic energies within the 15 keV and 15 MeV range. The densities and elemental compositions of the samples were used as the input data in the mentioned computational software.

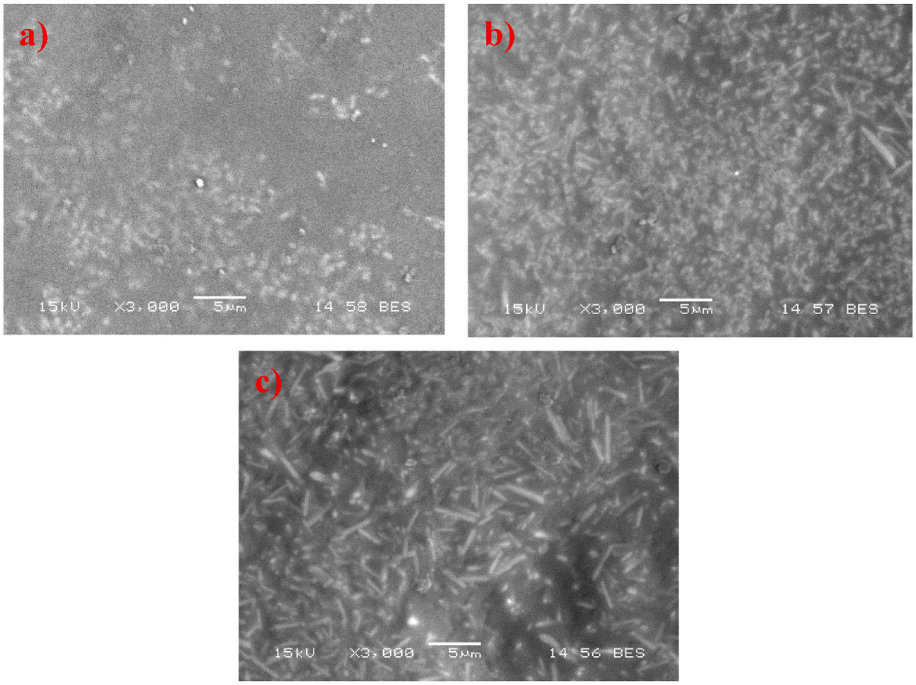

Fig. 2. SEM images of the GC samples a) AW b) AW-B10 c) AW-B20.

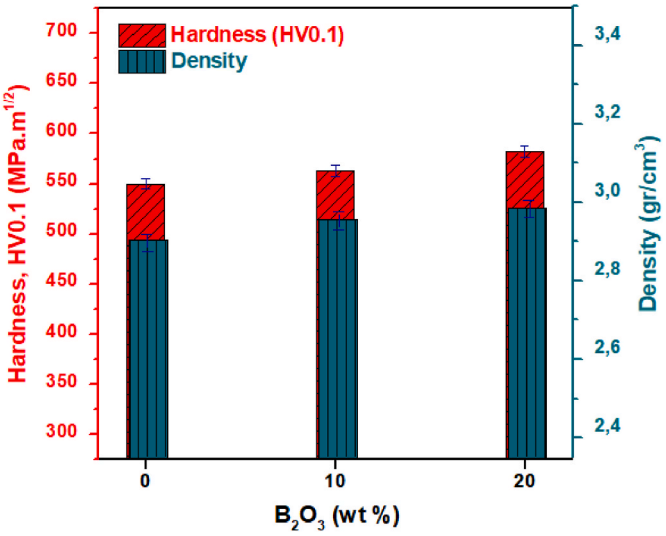

Fig. 3. The relationship between hardness and density depending on B_2O_3 content.

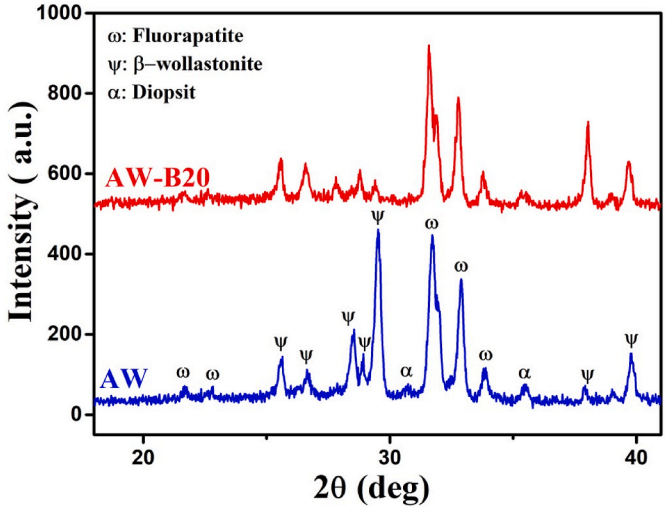

Fig. 4. XRD spectrogram of AW and AW-B20.

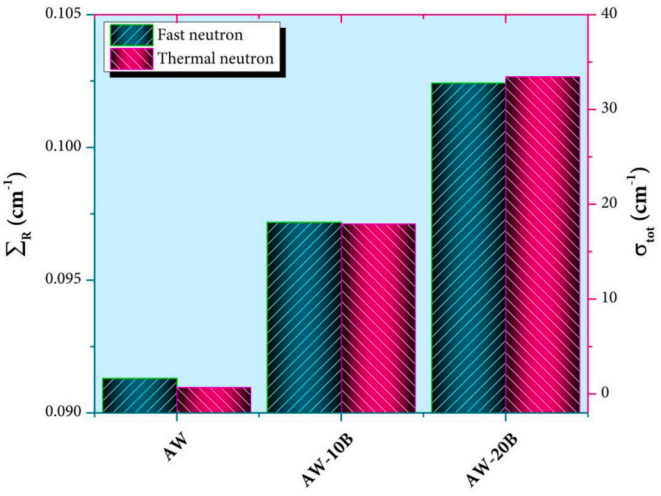

Fig. 5. Variation of removal and total scattering cross sections of the prepared AW-*x*B glasses for fast and thermal neutrons.

3. Results and discussion

3.1. Chemical analysis and density

The results of the chemical analysis of the GC samples as well as the measured density are presented in Table 2. The undoped AW sample can be seen to consist of oxides of Ca, Si, P, Mg, and Al. The trace amount of F in the sample was present in the form of CaF_2. In the absence of Al, the chemical distribution of elements is similar to those of Kokubo et al. and previously reported AW samples [10,29–32]. The presence of Al in the samples could be attributed to impurities from the milling and calcination processes. In addition, the introduction of B_2O_3, as expected, reduced the weight concentrations of the oxides present in the AW sample. Doping AW with B_2O_3 gradually increased the density of the GCs, as seen in Table 2. The density of AW (2.905 gcm^{-3}) increases to about 2.957 and 2.986 gcm^{-3} as B_2O_3 increases to 10 and 20 wt%, respectively. This suggests better compatibility and strength for samples rich in B_2O_3. Comparatively, the density of the AW and B_2O_3-doped AW GCs are higher than those of some common glasses, including soda-lime (2.40 gcm^{-3}), silicate (2.18 gcm^{-3}), and borosilicate (2.23 gcm^{-3}) glasses [32,33]. Also, compared to Li_2O (2.12–2.29 gcm^{-3}), Na_2O (2.21–2.47 gcm^{-3}, and K_2O (2.14–2.38 gcm^{-3}) -doped borate glasses [34], the densities of the B_2O_3-doped AW GCs are higher. This could be an indication of higher compactness and mechanical strength simulated by the presence of the AW crystal structure. On the other hand, the density pristine AW sample (2.905 gcm^{-3}) had comparable density (2.917 gcm^{-3}) with AW sample prepared in previous study [32]. The slim differences in the two densities could be attributed to nearly similar chemical composition of the two undoped AW samples.

3.2. Surface and crystal structure

The SEM images of the produced AW-doped samples are presented in Fig. 2. The white regions in Fig. 2(a) show fine-grained apatite crystals. The absence of pores in the structure is an indication of condensation. Apatite crystals in the structure are almost spherical. When Fig. 2 (b) is examined, it is seen that the number of apatite crystals increased with the addition of B_2O_3. As the B_2O_3 contribution increases (Fig. 2(c)), it is observed that the apatite crystals condense and become homogeneous. In addition, it is seen that the crystals started to transform from spherical form to rod form. The presence of B_2O_3 thus supported the formation and growth of apatite crystals. The Vickers hardness values were calculated as 550, 563 and 582 HV under a 0.1 kg load for AW, AW-10B, and AW-20B, respectively. As shown in Fig. 3, the B_2O_3-rich AW GCs samples have higher Vickers hardness values. Also, the density of the GCs increased as the B_2O_3 content increased. The calculated densities are 2.905, 2.957, and 2.986 g/cm^3 for the AW, AW-10B, and AW-20B, respectively. The increase in GCs density and hardness indicates that doping AW with B_2O_3 increases its compactness and strength. The higher hardness of the B_2O_3-rich glass could be attributed to the increase in the formation of fine and fibrous microstructure within the GCs system. The XRD spectrogram in Fig. 4 supports the predominance of apatite crystals in the presence of B_2O_3, thus complementing the observation of the SEM images. It appears that the presence of boron oxide supported the wollastonite phase to remain glass and suppressed crystallisation.

3.3. Radiation interaction property

Radiation interaction parameters are important for delineating materials for application in radiation environments. They are also crucial for identifying radiation dosimetry potentials and shielding competence a substance possesses. For AW GCs, they are important radiological studies of tissues and substitute materials. The value of Σ_R and the parameters adopted in estimating it for the GCs are presented in Fig. 5. The

Table 3
The FN moderating capacity of AW-B20 in contrast. to different categories of moderators.

Material	$\Sigma_R\,(cm^{-1})$	Reference
AW-20B	0.1024	Present Study
Graphite	0.0771	[35]
Water	0.1024	[36]
Ordinary concrete (OC)	0.0937	[37]
Hematite-serpentine concrete (HSC)	0.0967	
Ilmenite-limonite concrete (ILC)	0.095	
Basalt-magnetite concrete (BMC)	0.1102	
Steel-magnetite concrete (SMC)	0.142	
PA-6 polymer	0.1151	[38]
PVDC polymer	0.0706	
SSS30 glass	0.0893	[39]
B4 glass	0.092	[40]
G5 glass	0.1055	
L5 glass	0.1123	
S5 glass	0.0985	
CoO-4	0.0959	[41]
NiO–4C	0.0997	[42]
ICSW9	0.0916	[43]
3%V–B3	0.0979	[44]
FBCSP4 alloy	0.1561	[45]

values of the FN removal probabilities for AW, AW-B10, and AW-B20 are 0.0913 cm^{-1}, 0.0972 cm^{-1}, and 0.1024 cm^{-1}, respectively. These represent about 6.46 % and 12.16 % growth in the ability of the AW GCs to slow down FN as the boron (III) oxide weight proportion increases by 10 and 20 wt%, respectively. The rise in the value of Σ_R can be a result of higher values of ρ_i, $\left(\frac{\Sigma_R}{\rho}\right)_i$ or both, as predicted by Equation (1). A close look at Table 2 reveals that B and O have higher $\left(\frac{\Sigma_R}{\rho}\right)_i$ compared to other elements contained in the AW-Bx GCs. The introduction of B_2O_3 into AW increased the relative weight content and partial densities of B and O, while reducing those of other chemical species in the GCs system. This is responsible for the consistent growth in the value of Σ_R as displayed in Fig. 5. This shows that the FN thermalizing ability of B_2O_3-doped AW increases with B_2O_3 content. AW-B20 has Σ_R value is higher than that of some human tissues, such as cortical bone (0.0637 cm^{-1}), and the brain (0.1015 cm^{-1}). It is, however, lower than that of muscle (0.1032 cm^{-1}) and soft tissues (0.1047 cm^{-1}) [28]. The Σ_R could be used to predict which tissues respond in a similar way to FN interaction. In addition, the FN moderating capacity of AW-B20 is related to that of different classes of materials in Table 3. The classes of materials are traditional fast neutron moderators (graphite and water), light and heavy concrete (OC, HSC, ILC, BMC, and SMC), polymers (PA-6 and PVDC), shielding glasses (SSS30, B4, G5, L5, and S5), bioactive glasses (CoO-4, NiO–4C, ICSW9, and 3%V–B3), and a Fe-based alloy (FBCSP4). The table shows that AW-20B has a comparable FN neutron moderating capacity as water and a higher FN removal ability compared to many of the compared materials such as graphite, OC, HSC, ILC, PVDC, SSS30, B4, S5, CoO-4, NiO–4C, ICSW9, and 3%V–B3. This implies AW-20B is a better moderator compared to these materials. The relatively higher Σ_R value of AW-20B can be attributed to its high B content as well as other low-atomic-number elements.

Table 3 shows the total cross-sections as well as the interaction (scattering and absorption) of moderated neutrons. The data show that all the σ_j increase with B_2O_3 weight quantity in AW. The higher σ_j of B compared to other identified elements in the AW-Bx composition is the

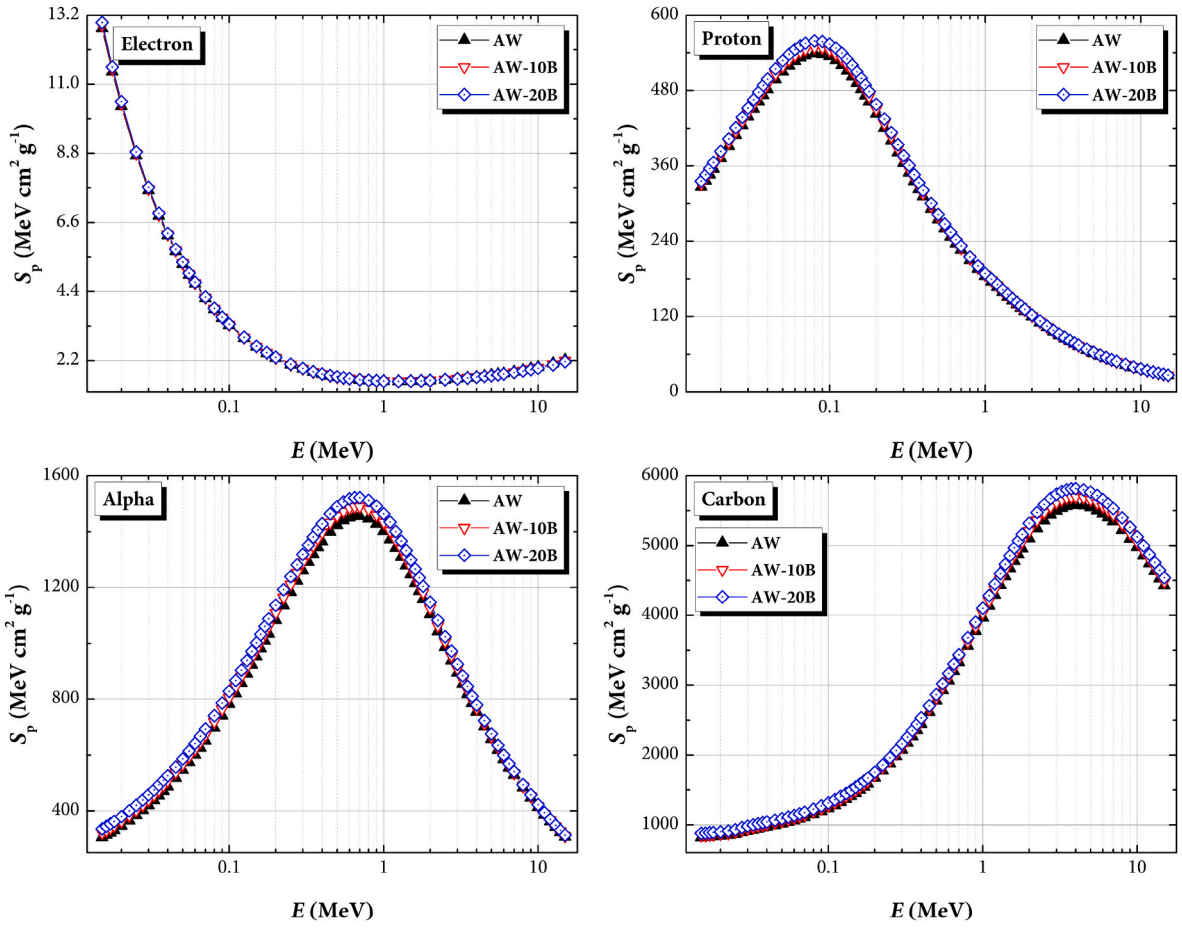

Fig. 6. Variations of total mass stopping power with respect to a function of kinetic energy in the prepared AW-*x*B glasses presented for electron, proton & alpha particles, and carbon ion.

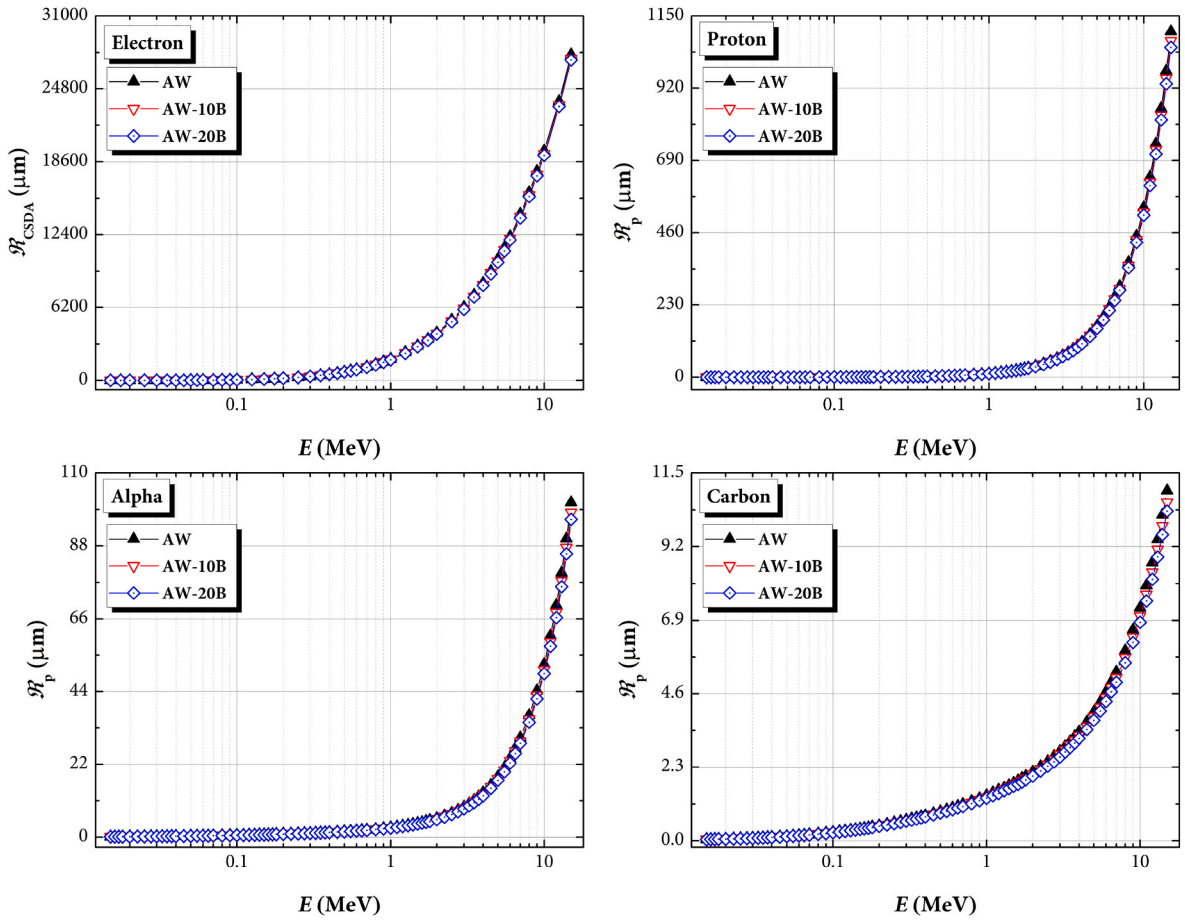

Fig. 7. Variations of range (ℜ) with respect to a function of kinetic energy in the prepared AW-*x*B glasses presented for electron, proton & alpha particles, and carbon ion.

factor responsible for the steady growth of the scattering, absorption and total σ_j (as seen in Fig. 5). Also, the σ_{tot} value of AW-20B is greater than that of B4 (2.847 cm^{-1}), L5 (25.5 cm^{-1}), and S5 (17.244 cm^{-1}) glasses [40]; an indication of better thermal neutron interaction competence relative to the glasses. The addition of B to AW increased the thermal neutron cross-sections considerably. It is safe to conclude that increasing the amount of B_2O_3 in AW can be used to improve the FN and thermal neutron interaction probabilities. The B-rich AW is thus potentially useful as a target material in human tissues for boron neutron capture therapy for the management of cancer and tumours.

The stopping power and range of charged radiation (CR) or ions are important in many areas of radiation physics, such as shielding design, absorbed energy calculation, and radiation-induced damage estimation, among others. Due to the use of radiation in many fields, including medicine, the S_p and ranges of some common ions or CR encountered in radiation therapy is important. The S_p electrons, protons, apha particles, and carbon ions in AW, AW-B10, and AW-B20 are plotted against particle kinetic energy (T) between 15 and 15000 keV and shown in Fig. 6. For AW, the S_p electrons, protons, α-particles, and carbon ions were within the ranges of 1.54–12.78 $MeVcm^2g^{-1}$, 26.42–539.06 $MeVcm^2g^{-1}$, 305.34–1455.51 $MeVcm^2g^{-1}$, and 820.80–5583.45 $MeVcm^2g^{-1}$, respectively. For AW-B10, the ranges are 1.54–12.88 $MeVcm^2g^{-1}$, 26.59–548.97 $MeVcm^2g^{-1}$, 320.51–1488.52 $MeVcm^2g^{-1}$, and 848.70–5699.50 $MeVcm^2g^{-1}$, while for AW-B20 they are 1.54–12.97 $MeVcm^2g^{-1}$, 26.78–558.98 $MeVcm^2g^{-1}$, 335.68–1521.54 $MeVcm^2g^{-1}$, and 876.6–5800.36 $MeVcm^2g^{-1}$, accordingly. Generally, CR interacts with matter through Coulomb interactions and nuclear collisions. The energy dependence of S_p varies for each ion depending of the particle properties, such as charge and energy, and the interacting medium effective electron density. Empirically, S_p is given as [45,46]:

$$S_p\left(MeVcm^2g^{-1}\right) = 2C\left\{\ln\left(\frac{\left(1.02\times10^6\times\beta^2\right)}{I\left(1-\beta^2\right)}\right)-\beta^2\right\} \tag{7}$$

$$C\left(MeVcm^2g^{-1}\right) = \frac{0.154z^2\left(Z/A\right)}{\beta^2} \tag{8}$$

where, β is the normalised incident particle velocity, Z/A is the number of electrons per unit molar mass of the interacting medium, and I is the Z-dependent ionisation potential of the absorber. Higher S_p values are expected for particles with a higher charge magnitude (z^2). This is due to the higher Coulomb interaction losses. In addition, materials with higher Z/A values are expected to have higher S_p. This means they slow down charged radiation at a faster rate per unit mass thickness. Based on the values of the stopping powers, it is clear that the increase in the B_2O_3 content enhances the S_p of the GCs. Comparatively, the S_p of the AW at each energy trends according to the following order: $(S_p)^{AW} < (S_p)^{AW-10} < (S_p)^{AW-B20}$.

As a charged particle moves in matter, it slows down due to energy loss. If the interacting medium is thick enough, the particle would eventually lose all its energy and come to rest in the medium. The projected range (ℜ) measures how far the particle moved before losing all its energy. Fig. 6 shows a plot of the range of the four CR considered in this work for the three doped AW GCs. The decreasing interacting probabilities of more energetic particles ensure they travel farther in a given substance. Therefore, Fig. 7 shows that the range of each radiation

type increases with particle kinetic energy. Also, B_2O_3 makes the AW less transparent to CR as the particle range is reduced in B-rich AW samples. For example, for 15 MeV carbon ions, the ranges in AW, AW-B10, and AW-B20 are 10.95 μm, 10.59 μm, and 10.31 μm, respectively. The B-rich AW could thus be used for isolating or shielding specific tissues in ion beam therapy processes and other techniques that require the exposure of human tissues to ion beam irradiation [47–51]. This will ensure radiation or particles are retained within the target volume using tissue-compatible biomaterials or glassy materials[52,53].

4. Conclusion

In this research, the synthesis, structural and microstructural properties, physical features, and neutron, light, and heavy ion cross-section-related parameters of AW GCs are reported. The density of the GCs increased, suggesting better compatibility and strength for B_2O_3-rich AW GCs. The introduction of boron oxide supported the wollastonite phase to remain glass and suppressed crystallisation. The values of the FN removal probabilities for AW, AW-B10, and AW-B20 are 0.0913 cm^{-1}, 0.0972 cm^{-1}, and 0.1024 cm^{-1}, respectively. The results of the neutron cross-sections showed that B_2O_3 in AW can be used to improve the FN and thermal neutron interaction probabilities. The S_p values of the AW at each energy and charged radiation trend according to the order: $(S_p)^{AW} < (S_p)^{AW-10} < (S_p)^{AW-B20}$. Also, B_2O_3 makes the AW less transparent to CR as the particle range is reduced in B-rich AW samples. The B-rich AW could find applications in neutron and ion beam therapy as a radiation absorber outside target volumes. However, the long-term stability in human tissues or the environment against radiation would need to be verified before practical deployment.

Declaration of competing interest

All authors must disclose any financial and personal relationships with other people or organizations that could inappropriately influence (bias) their work or state if there are no interests to declare.

Acknowledgement

The authors express their gratitude to Princess Nourah bint Abdulrahman University Researchers Supporting Project number (PNURSP2024R26), Princess Nourah bint Abdulrahman University, Riyadh, Saudi Arabia.

References

[1] R.G. Ribas, V.M. Schatkoski, T.L. do Amaral Montanheiro, B.R.C. de Menezes, C. Stegemann, D.M.G. Leite, G.P. Thim, Current advances in bone tissue engineering concerning ceramic and bioglass scaffolds: a review, Ceram. Int. 45 (17) (2019) 21051–21061.
[2] J. Massera, Bioactive glass-ceramics: from macro to nano, in: Nanostructured Biomaterials for Regenerative Medicine, Woodhead Publishing, 2020, pp. 275–292.
[3] D.G. Filip, V.A. Surdu, A.V. Paduraru, E. Andronescu, Current development in biomaterials—hydroxyapatite and bioglass for applications in biomedical field: a review, J. Funct. Biomater. 13 (4) (2022) 248.
[4] S. Singh, A. Patil, S. Mali, H. Jaiswal, Bioglass: a new era in modern dentistry, European J. General Dentist. 11 (1) (2022) 1–6.
[5] S. Dasgupta, S.S. Banerjee, A. Bandyopadhyay, S. Bose, Zn-and Mg-doped hydroxyapatite nanoparticles for controlled release of protein, Langmuir 26 (7) (2010) 4958–4964.
[6] S.W. Tsai, S.S. Huang, W.X. Yu, Y.W. Hsu, F.Y. Hsu, Fabrication and characteristics of porous hydroxyapatite-CaO composite nanofibers for biomedical applications, Nanomaterials 8 (8) (2018) 570.
[7] A. Pistone, D. Iannazzo, C. Espro, S. Galvagno, A. Tampieri, M. Montesi, M. Sandri, Tethering of Gly-Arg-Gly-Asp-Ser-Pro-Lys peptides on Mg-doped hydroxyapatite, Engineering 3 (1) (2017) 55–59.
[8] M. Magallanes-Perdomo, Z.B. Luklinska, A.H. De Aza, R.G. Carrodeguas, S. De Aza, P. Pena, Bone-like forming ability of apatite–wollastonite glass ceramic, J. Eur. Ceram. Soc. 31 (9) (2011) 1549–1561.
[9] A.B. Workie, H.S. Ningsih, W.L. Yeh, S.J. Shih, An investigation of in vitro bioactivities and cytotoxicities of spray pyrolyzed apatite wollastonite glass-ceramics, Crystals 13 (7) (2023) 1049.
[10] T. Kokubo, M. Shigematsu, Y. Nagashima, M. Tashiro, T. Nakamura, T. Yamamuro, S. Higashi, Apatite-and wollastonite containg glass-ceramics for prosthetic application, Bull. Inst. Chem. Res. Kyoto Univ. 60 (1982) 260–268.
[11] E.A. Abou Neel, W. Chrzanowski, D.M. Pickup, L.A. O'Dell, N.J. Mordan, R. J. Newport, J.C. Knowles, Structure and properties of strontium-doped phosphate-based glasses, J. R. Soc. Interface 6 (34) (2009) 435–446.
[12] M. Miola, C.V. Brovarone, G. Maina, F. Rossi, L. Bergandi, D. Ghigo, E. Vernè, In vitro study of manganese-doped bioactive glasses for bone regeneration, Mater. Sci. Eng. C 38 (2014) 107–118.
[13] S. Murphy, D. Boyd, S. Moane, M. Bennett, The effect of composition on ion release from Ca–Sr–Na–Zn–Si glass bone grafts, J. Mater. Sci. Mater. Med. 20 (2009) 2207–2214.
[14] O.P. Filho, G.P. La Torre, L.L. Hench, Effect of crystallization on apatite-layer formation of bioactive glass 45S5, J. Biomed. Mater. Res.: Off. J. Soc. Biomater. Japanese Soc. Biomater. 30 (4) (1996) 509–514.
[15] P. Melo, M. Kotlarz, M. Marshall, M. Magallanes, A.M. Ferreira, P. Gentile, K. Dalgarno, Effects of alumina on the thermal processing of apatite-wollastonite: changes in sintering, microstructure and crystallinity of compressed pellets, J. Eur. Ceram. Soc. 40 (15) (2020) 6107–6113.
[16] Jing, H., Gan, T., Tang, X., & Li, F. Effect of Titanium Addition on Physicochemical and Biological Properties of Apatite-Wollastonite Glass Ceramic..
[17] A. Evcin, B. Büyükleblebici, Ti6Al4V coating with B 2 O 3 and Al 2 O 3 containing hydroxyapatite by HVOF technique, Scientia Iranica. Transact. Nanotechnol. 26 (3) (2019) 1980–1989.
[18] X. Yang, L. Zhang, X. Chen, X. Sun, G. Yang, X. Guo, Z. Gou, Incorporation of B2O3 in CaO-SiO2-P2O5 bioactive glass system for improving strength of low-temperature co-fired porous glass ceramics, J. Non-Cryst. Solids 358 (9) (2012) 1171–1179.
[19] A. Saranti, I. Koutselas, M.A. Karakassides, Bioactive glasses in the system CaO–B2O3–P2O5: preparation, structural study and in vitro evaluation, J. Non-Cryst. Solids 352 (5) (2006) 390–398.
[20] J.H. Lee, C.K. Lee, B.S. Chang, H.S. Ryu, J.H. Seo, K.S. Hong, H. Kim, In vivo study of novel biodegradable and osteoconductive CaO-SiO2-B2O3 glass-ceramics, J. Biomed. Mater. Res. Part A: An Official Journal of The Society for Biomaterials, The Japanese Society for Biomaterials, and The Australian Society for Biomaterials and the Korean Society for Biomaterials 77 (2) (2006) 362–369.
[21] H.S. Ryu, J.K. Lee, J.H. Seo, H. Kim, K.S. Hong, D.J. Kim, S.S. Chung, Novel bioactive and biodegradable glass ceramics with high mechanical strength in the CaO SiO2 B2O3 system, J. Biomed. Mater. Res. Part A: An Official Journal of The Society for Biomaterials, The Japanese Society for Biomaterials, and The Australian Society for Biomaterials and the Korean Society for Biomaterials 68 (1) (2004) 79–89.
[22] N.A. Elsheikh, Gamma-ray and neutron shielding features for some fast neutron moderators of interest in 252Cf-based boron neutron capture therapy, Appl. Radiat. Isot. 156 (2020) 109012.
[23] Y.S. Rammah, F.I. El-Agawany, A. Gamal, I.O. Olarinoye, E.M. Ahmed, A. S. Abouhaswa, Responsibility of Bi2O3 content in photon, alpha, proton, fast and thermal neutron shielding capacity and elastic moduli of ZnO/B2O3/Bi2O3 glasses, J. Inorg. Organomet. Polym. Mater. 31 (8) (2021) 3505–3524.
[24] T. Piotrowski, Neutron shielding evaluation of concretes and mortars: a review, Construct. Build. Mater. 277 (2021) 122238.
[25] I.O. Olarinoye, F.I. El-Agawany, A. El-Adawy, Y.S. Rammah, Mechanical features, alpha particles, photon, proton, and neutron interaction parameters of TeO2–V2O3–MoO3 semiconductor glasses, Ceram. Int. 46 (14) (2020) 23134–23144.
[26] J.F. Ziegler, M.D. Ziegler, J.P. Biersack, SRIM–The stopping and range of ions in matter (2010), Nucl. Instrum. Methods Phys. Res. Sect. B Beam Interact. Mater. Atoms 268 (11–12) (2010) 1818–1823.
[27] M.J. Berger, ESTAR, PSTAR, ASTAR. A PC Package for Calculating Stopping Powers and Ranges of Electrons, Protons and Helium Ions, International Atomic Energy Agency, 1993. Version 2 (No. IAEA-NDS–144).
[28] W.H. Jin, C. Seldon, M. Butkus, W. Sauerwein, H.B. Giap, A review of boron neutron capture therapy: its history and current challenges, Int. J. Particle Ther. 9 (1) (2022) 71–82.
[29] T. Kokubo, Bioactive glass ceramics: properties and applications, Biomaterials 12 (2) (1991) 155–163.
[30] T. Kitsugi, T. Yamamuro, T. Nakamura, T. Kokubo, Bone bonding behavior of MgO CaO SiO2 P2O5 CaF2 glass (mother glass of A· W-glass-ceramics), J. Biomed. Mater. Res. 23 (6) (1989) 631–648.
[31] T. Kokubo, S. Ito, Z.T. Huang, T. Hayashi, S. Sakka, T. Kitsugi, T. Yamamuro, Ca, P-rich layer formed on high-strength bioactive glass-ceramic A-W, J. Biomed. Mater. Res. 24 (3) (1990) 331–343.
[32] V. Cannillo, F. Pierli, S. Sampath, C. Siligardi, Thermal and physical characterisation of apatite/wollastonite bioactive glass–ceramics, J. Eur. Ceram. Soc. 29 (4) (2009) 611–619.
[33] H. Rawson, Properties and applications of glasses, in: Glass Science and Technology, vol. 3, Elsevier, Amsterdam, 1980.
[34] H. Doweidar, G.M. El-Damrawi, Y.M. Moustafa, R.M. Ramadan, Density of mixed alkali borate glasses: a structural analysis, Phys. B Condens. Matter 362 (1–4) (2005) 123–132.
[35] R. El-Mallawany, F.I. El-Agawany, M.S. Al-Buriahi, C. Muthuwong, A. Novatski, Y. S. Rammah, Optical properties and nuclear radiation shielding capacity of TeO2-Li2O-ZnO glasses, Opt. Mater. 106 (2020) 109988.
[36] M.S. Al-Buriahi, A.S. Abouhaswa, H.O. Tekin, C. Sriwunkum, F.I. El-Agawany, T. Nutaro, Y.S. Rammah, Structure, optical, gamma-ray and neutron shielding

properties of NiO doped B2O3–BaCO3–Li2O3 glass systems, Ceram. Int. 46 (2) (2020) 1711–1721.
[37] I.I. Bashter, Calculation of radiation attenuation coefficients for shielding concretes, Ann. Nucl. Energy 24 (17) (1997) 1389–1401.
[38] M.R. Kaçal, F. Akman, M.I. Sayyed, Evaluation of gamma-ray and neutron attenuation properties of some polymers, Nucl. Eng. Technol. 51 (3) (2019) 818–824.
[39] F.I. El-Agawany, O.L. Tashlykov, K.A. Mahmoud, Y.S. Rammah, The radiation-shielding properties of ternary SiO2–SnO–SnF2 glasses: simulation and theoretical study, Ceram. Int. 46 (15) (2020) 23369–23378.
[40] G. Lakshminarayana, H.O. Tekin, M.G. Dong, M.S. Al-Buriahi, D.E. Lee, J. Yoon, T. Park, Comparative assessment of fast and thermal neutrons and gamma radiation protection qualities combined with mechanical factors of different borate-based glass systems, Results Phys. 37 (2022) 105527.
[41] H.O. Tekin, E. Kavaz, E.E. Altunsoy, O. Kilicoglu, O. Agar, T.T. Erguzel, M. I. Sayyed, An extensive investigation on gamma-ray and neutron attenuation parameters of cobalt oxide and nickel oxide substituted bioactive glasses, Ceram. Int. 45 (8) (2019) 9934–9949.
[42] H.O. Tekin, O. Kilicoglu, Esra Kavaz, E. Esra Altunsoy, M. Almatari, O. Agar, M. I. Sayyed, The investigation of gamma-ray and neutron shielding parameters of Na2O-CaO-P2O5-SiO2 bioactive glasses using MCNPX code, Results Phys. 12 (2019) 1797–1804.
[43] A.M. Deliormanlı, M.S. Al-Buriahi, H.H. Somaily, H.O. Tekin, 13-93B3 Bioactive glasses containing Ce 3+, Ga 3+ and V 5+: dose rate and gamma radiation characteristic for medical purposes, Appl. Phys. A 127 (2021) 1–14.
[44] B. Alshahrani, I.O. Olarinoye, C. Mutuwong, C. Sriwunkum, H.A. Yakout, H. O. Tekin, M.S. Al-Buriahi, Amorphous alloys with high Fe content for radiation shielding applications, Radiat. Phys. Chem. 183 (2021) 109386.
[45] M.S. Al-Buriahi, J.S. Alzahrani, I.O. Olarinoye, H. Akyildirim, S. Alomairy, I. Kebaili, C. Mutuwong, Role of heavy metal oxides on the radiation attenuation properties of newly developed TBBE-X glasses by computational methods, Phys. Scripta 96 (7) (2021) 075302.
[46] N. Tsoulfanidis, S. Landsberger, O. Gayou, Measurement and detection of radiation, Med. Phys. 39 (7) (2012) 4618.
[47] Ozge Kilicoglu, H.O. Tekin, Bioactive glasses and direct effect of increased K2O additive for nuclear shielding performance: a comparative investigation, Ceram. Int. 46 (2) (2020) 1323–1333.
[48] Aylin M. Deliormanli, Shams AM. Issa, M.S. Al-Buriahi, Begüm Rahman, Hesham MH. Zakaly, H.O. Tekin, Erbium (III)-and Terbium (III)-containing silicate-based bioactive glass powders: physical, structural and nuclear radiation shielding characteristics, Appl. Phys. A 127 (6) (2021) 463.
[49] H.O. Tekin, M.S. Al-Buriahi, Shams AM. Issa, Hesham MH. Zakaly, Bashar Issa, Imen Kebaili, Badawi Ali, M.K.A. Karim, K.A. Matori, M.H.M. Zaid, Effect of Ag2O substituted in bioactive glasses: a synergistic relationship between antibacterial zone and radiation attenuation properties, J. Mater. Res. Technol. 13 (2021) 2194–2201.
[50] Aylin M. Deliormanlı, Mertcan Ensoylu, Shams AM. Issa, Wiam Elshami, Ateyyah M. Al-Baradi, M.S. Al-Buriahi, H.O. Tekin, WS2/bioactive glass composites: fabrication, structural, mechanical and radiation attenuation properties, Ceram. Int. 47 (21) (2021) 29739–29747.
[51] G. Lakshminarayana, Ashok Kumar, H.O. Tekin, AM Issa Shams, M.S. Al-Buriahi, Dong-Eun Lee, Jonghun Yoon, Taejoon Park, Binary B2O3–Bi2O3 glasses: scrutinization of directly and indirectly ionizing radiations shielding abilities, J. Mater. Res. Technol. 9 (6) (2020) 14549–14567.
[52] M.S. Al-Buriahi, Radiation shielding performance of a borate-based glass system doped with bismuth oxide, Radiation Physics and Chemistry 207 (2023) 110875.
[53] Al-Buriahi, Mohammed Sultan, Halil Arslan, H. O. Tekin, V. P. Singh, and Baris T. Tonguc. "MoO3-TeO2 glass system for gamma ray shielding applications." *Materials Research Express* 7, no. 2 (2020): 025202.